AUGUST 1981

PPPL-1822
UC-20G

AN ENHANCED-CONFINEMENT CLASS OF STELLARATORS

BY

H.E. MYNICK, T.K. CHU AND A.H. BOOZER

PLASMA PHYSICS LABORATORY

PRINCETON UNIVERSITY
PRINCETON, NEW JERSEY

This work supported by the U.S. Department of Energy Contract No. DE-AC02-76-CHO-3073. Reproduction, translation, publication, use and disposal, in whole or in part, by or for the United States Government is permitted.

An Enhanced-Confinement Class of Stellarators

H. E. Mynick, T. K. Chu, and A. H. Boozer

Princeton Plasma Physics Laboratory

Princeton University

Princeton, New Jersey 08544

Abstract

A class of stellarators has been found in which the transport is reduced by an order of magnitude from transport in conventional stellarators, by localizing the helical ripple to the inside of the torus. The reduction is observed in numerical experiments and explained theoretically.

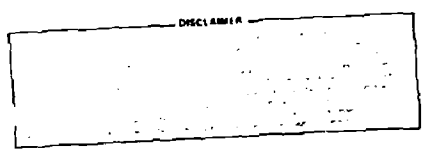

We here report on the discovery of a family of stellarator configurations having transport which is greatly reduced from that which has been theoretically predicted [1,2] and observed in numerical experiments,[3] for the standard configuration traditionally envisioned. Such an enhancement of confinement is important, since the transport levels predicted by the theory of Refs. 1 and 2 may be too large to make a reactor of acceptable size.

The new configurations are related to one proposed by Meyer and Schmidt[4] (the "M-S" configuration). There, the objective was to improve the equilibrium properties at high β (the ratio of the pressures of the plasma and the confining magnetic field) by reducing the Pfirsch-Schluter currents J_{ps}. This is achieved by localizing the ripple in the magnetic field $\underset{\sim}{B}$ induced by the helical windings to the inside of the torus (poloidal angle θ near π), in such a way that the Fourier component of $B \equiv |\underset{\sim}{B}|$ at $\cos\theta$, which gives rise to J_{ps}, is approximately eliminated. The present class of stellarators shares with the M-S configuration the localization of the helical ripple to the inside of the torus. However, the $\cos\theta$ component of B must <u>not</u> be eliminated; its optimum size will be discussed later in this paper.

Realizations of the configuration are obtainable using modular coils, and members of this class have been found[5] which possess a minimum average - B magnetic well. One may thus expect such configurations to possess good MHD stability properties.

Numerical results for stellarator transport have previously been obtained, showing slightly better[6] or dramatically better[7] confinement at low collision frequency ν than that predicted theoretically. However, the origin of this improved confinement was not understood. In Ref. 3 (where the theoretical predictions were <u>confirmed</u> numerically), it was argued that, while one might question aspects of the numerical and statistical procedure in Ref.

7, part of the explanation for the very favorable numerical results obtained there could lie in the richer harmonic content of $B(r,\phi,\theta)$ over a flux surface (r = cst). The configurations investigated here are one example of improving transport through more complex structure of B, and the physical mechanism for the improvement is described here.

Description of the Configuration

We adopt a coordinate system natural to the magnetic geometry. We use the flux function ψ as the radial coordinate, satisfying $\underset{\sim}{B}\cdot\underset{\sim}{\nabla}\psi = 0$, or equivalently, a radial variable $r(\psi)$ having units of length, defined by $\psi = 1/2\ B_o\ r^2$, with B_o the toroidal field strength on the magnetic axis. Each ψ-surface is parameterized by poloidal angle θ and toroidal angle ϕ, chosen so that the rotational transform $q^{-1} \equiv d\theta/d\phi$ of a field line is a function of ψ only. The guiding-center equations of motion in these coordinates are then given, once a description for field strength $B(r,\phi,\theta)$ is specified.[6] We compare three configurations here, designated by configuration index $\sigma = 0, \pm 1$, given for all r by

$$B(r,\phi,\theta) = B_o\left[1 - \varepsilon_t\cos\theta - \varepsilon_h\cos\eta + \frac{1}{2}\,\sigma(\varepsilon_{h-}\cos\eta_- + \varepsilon_{h+}\cos\eta_+)\right] . \qquad (1)$$

Here $\eta \equiv \ell\theta - m\phi$, $\eta_\pm \equiv \ell_\pm\theta - m\phi$, $\ell_\pm \equiv \ell \pm 1$, $\varepsilon_h(r) \propto r^{\ell}$, $\varepsilon_h(r) \propto r^{\ell_\pm}$, $\varepsilon_t(r) \equiv r/R_o \equiv \varepsilon_a r/a$ is the inverse aspect ratio, and a is the value of r at the plasma edge. The standard configuration of Refs. 1, 2, and 3 is given by $\sigma = 0$. At a particular value r_1 of r, $\varepsilon_{h\pm}$ are chosen to satisfy $\varepsilon_h(r_1) =$

$\varepsilon_{h+}(r_1) = \varepsilon_{h-}(r_1)$. Then Eq. (1) takes the simpler form

$$B(r,\phi,\theta) = B_o\left[1 - \varepsilon_t\cos\theta - \varepsilon_h\cos\eta(1 - \sigma\cos\theta)\right] \quad , \tag{2}$$

where the modulating envelope $(1 - \sigma\cos\theta)$ localizes the ripple to the interior (exterior) of the torus, for $\sigma = 1(-1)$. The $\sigma = 1$ configuration is the one with improved confinement; the -1 configuration has very poor confinement, and is studied to help discern the physical origin of the improvement for $\sigma = 1$.

In Figs. 1(a), (b), and (c) are shown profiles of B along a field line for $\sigma = 0$, 1, and -1, respectively, for $\ell = 2$, $m = 6$, $q^{-1} = .3$, $\varepsilon_t = .05$, and $\varepsilon_h = \varepsilon_{h+} = \varepsilon_{h-} = .05$ at $r_1/a = .5$. The flat-bottomed appearance of the $\sigma = 1$ B envelope is the result of the particular choice $p \equiv \varepsilon_h/\varepsilon_t = 1$ we take for the transport results shown here; this is not a necessary, nor even optimal, value for p.

Particle Orbits

In the numerical results to be presented shortly, the $\sigma = 1$ configuration shows much better confinement than the $\sigma = 0$ or -1 configuration. The most important reason for this is that, for almost all helically-trapped particles, the contribution to the radial drift $\dot{r}$ coming from the $(1 - \cos\theta)$ modulation of ε_h cancels the toroidal contribution (cf. Eq. 3). This configuration, thus has drifts which can approach being omnigenous[8] (i.e. having $\dot{r} = 0$), for the most troublesome particles in the 0-configuration.

For these particles, the drifts normal to $\hat{B} \equiv \underset{\sim}{B}/B$ are dominated by the grad-B drift $\underset{\sim}{v}_B = (\mu/m\Omega)\,\hat{B} \times \underset{\sim}{\nabla}B$, where $\mu \equiv \left(mv_\perp^2/2\,B\right)$ is the particle's

magnetic moment, and $\Omega \equiv eB/mc$ is its gyrofrequency. (Here and throughout, we assume there are no electic fields, which may also have a beneficial effect on confinement.) Assuming $\hat{B} \approx \hat{\phi}$, using Eq. (1) near $r = r_1$ to compute $\underset{\sim}{\nabla}B$, and averaging over a helical bounce period τ_b, one obtains the drifts in the r and θ directions:

$$\dot{r} = v_{Bt} \sin\theta \, (1 - \sigma \, p \, \overline{\cos\eta}) \quad , \tag{3}$$

$$\Omega_\theta \equiv \dot{\theta} = v_{Bt} \left[\cos\theta + \ell p (1 - \sigma \cos\theta) \, \overline{\cos\eta} \, \right] / r \quad . \tag{4}$$

Here $v_{Bt} \equiv (\mu \varepsilon_t / m\Omega r)$ is the toroidal contribution to v_B, and the overbar denotes the average over τ_b. For $\sigma = \pm 1$, one sees from Eq. (3) that the radial drifts are modified, due to the $(1 - \sigma \cos\theta)$ modulation of ε_h.

For $\sigma \, p \, \overline{\cos\eta} = 1$, the drifts are fully omnigenous. The function $\overline{\cos\eta}(x)$ is plotted in Fig. 2 as a function of particle depth $x \equiv E_{\parallel b}/E_{\parallel mx}$ in a helical well. (Here $E_{\parallel b}$ is the parallel energy of a particle at the well bottom, and $E_{\parallel mx}$ is the maximum $E_\parallel$ a trapped particle can have in that well.) For deeply-trapped particles ($x = 0$), $\overline{\cos\eta}$ is near 1, and for all but the most shallowly-trapped, $\overline{\cos\eta}$ is positive, causing a reduction in $\dot{r}$ for $\sigma = 1$, and an enhancement for $\sigma = -1$.

The effect of this on particle orbits is illustrated by Figs. 3(a) and 3(b). These are poloidal projections of typical dominant contributors to the transport for their respective particle ensembles, for $\sigma = 1$ [Fig. 3(a)] and $\sigma = -1$ [Fig. 3(b)], at an initial radius for which $p \approx 1$. After the initial helical entrapment at point A in Fig. 3(a), the particle takes a fairly rapid radial step Δr_b, until it becomes deeply enough trapped to largely shut off $\dot{r}$. Thereafter, the drift motion is almost at constant r.

Numerical Results

In Fig. 4 are shown the results of numerical runs done using the guiding-center code with Monte-Carlo collision operator used in Refs. 3 and 6, for the $\sigma = 0, \pm 1$ configurations. As in Refs. 3 and 6, monoenergetic ensembles were used, started at initial radius $r/a = .5$, and randomly distributed in ϕ, θ, and pitch $\lambda \equiv v_\parallel/v$. For each value of collision frequency ν, an ensemble of 80 particle orbits was used, which gave a standard deviation in the diffusion coefficients $D(\nu)$ so obtained of about 20%.

We quote parameters in terms of units where $a = m = \Omega_o = 1$, with m the particle mass and $\Omega_o \equiv eB_o/mc$. In these units, a thermal ion with m = 2.5 amu in a reactor-regime plasma ($T_i = 8$ keV, $n_i = 10^{14}$ cm^{-3}, a = 2 m, B = 5 Tesla) will have collisionality $\nu \simeq \nu_R \equiv .6 \times 10^{-6}$ and energy $E = 1/2\ (\rho/a)^2 \simeq 1.7 \times 10^{-6}$. For these parameters a confinement time $\tau_E = a^2/4D$ of 1 second corresponds to a diffusion coefficient $D = D/a^2\Omega_o \simeq 1.25 \times 10^{-9}$.

For the results in Fig. 4, the parameters taken were the same as in Figs. 1, along with $E = 10^{-6}$. One sees that $D(\sigma = 1)$ is down from $D(\sigma = 0)$ and $D(\sigma = -1)$ by one and two orders of magnitude, respectively. A run time $T = 2/\nu_R = 3.33 \times 10^6$ was used for all orbits, independent of collision frequency ν. As pointed out in Ref. 3, for T less than the helical detrap time $\tau_h \equiv \epsilon_h/\nu$, the radial step Δr a trapped particle takes then becomes limited by a <u>numerical</u> time T rather than <u>physical</u> time τ_h, leading to a spuriously low value for D at lower ν. To this we attribute the fact that $D(\sigma = 0)$ in Fig. 4 lies appreciably below the theoretical prediction. This argument assumes, however, that T is also smaller than the time τ_r that a trapped particle moves radially during the full period τ_θ of a superbanana orbit. This is justified for $\sigma = 0$, where $\tau_r \sim \tau_\theta$, but not for $\sigma = 1$, where $\tau_r < T < \tau_\theta$, due to the short,

rapid radial step a trapped particle takes (Fig. 3a). Therefore, one may expect the numerical values given for $D(\sigma = 1)$ to be closer to the real values, at lower ν, than for $D(\sigma = 0, -1)$. In fact, test runs for longer T at $\nu \approx .003$ showed a slow increase in D for $\sigma \approx 0$, but <u>decrease</u> for $\sigma = 1$.

A kinetic-theoretical treatment of the transport valid for $\sigma = \pm 1$ (as well as $\sigma = 0$) is being developed, and will be presented elsewhere.[9] Here we quote a result of that theory, in the collisionality regime $\tau_b < \tau_h < \tau_r$. There, D is proportional to a positive definite integral I_x over pitch angle variable x, $I_x(\sigma p) = I_{00} - 2\sigma p I_{01} + (\sigma p)^2 I_{11}$, with $I_{00} = .3333$, $I_{01} = .2611$, and $I_{11} = .2079$. For $\sigma = 1$, one optimizes p by minimizing $I_x(p) \propto D$, finding $p_{opt} = I_{01}/I_{11} = 1.256$, at which value D is reduced from the $\sigma = 0$ value by a factor $I_x(p_{opt})/I_{00} \simeq (62.1)^{-1}$. For $p = 1$, the predicted reduction for this higher $-\nu$ regime is instead only $I_x(1)/I_{00} \simeq (17.5)^{-1}$, within a factor of two of the reduction found numerically.

Acknowledgments

This work supported by United States Department of Energy Contract No. DE-AC02-76-CH03073.

References

1. A. A. Galeev, R. Z. Sagdeev, H. P. Furth, and M. N. Rosenbluth, Phys. Rev. Lett. 22, 511 (1969).
2. J. W. Connor and R. J. Hastie, Phys. Fluids, 17, 114 (1974).
3. H. E. Mynick, PPPL Report # 1781 (1981) (submitted to Phys. Fluids).
4. F. Meyer, H. U. Schmidt, and Z. Naturforsch. 13a, 1005 (1958).
5. T. K. Chu, H. P. Furth, J. L. Johnson, C. Ludescher, and K. E. Weimer (private communications).
6. A. H. Boozer and G. Kuo-Petravic, Phys. Fluids, 24, 851 (1981).
7. R. E. Potok, P. A. Politzer, and L. M. Lidsky, Phys. Rev. Lett. 45, 1328 (1980).
8. L. S. Hall and B. McNamara, Phys. Fluids 18, 552 (1975).
9. H. E. Mynick (to be published).

Figure Captions

Fig. 1 Profiles of magnetic field strength along a field line for the three configurations studied.

Fig. 2 Plot of the bounce-averaged value of $\cos\eta$ as a function of well-depth parameter x. Particles trapped at the well bottom have $x = 0$, those barely trapped have $x = 1$.

Fig. 3 Poloidal projections of orbits characteristic of those contributing dominantly to the transport at low ν, for the $\sigma = 1$ (Fig. 3a) and $\sigma = -1$ (Fig. 3b) configurations. While the $\sigma = -1$ particle walks straight out of the device, once helically trapped, the $\sigma = 1$ particle has nearly omnigenous drifts, except for immediately after entrapping helically.

Fig. 4 Numerically-obtained transport results, for the $\sigma = 0, \pm 1$ configurations, for parameters given in the text. The numerical points for each σ are connected by solid line segments. The dashed lines show the theoretical predictions for the helical or superbanana (D_h) and tokamak-neoclassical (D_{nc}) contributions to the transport.

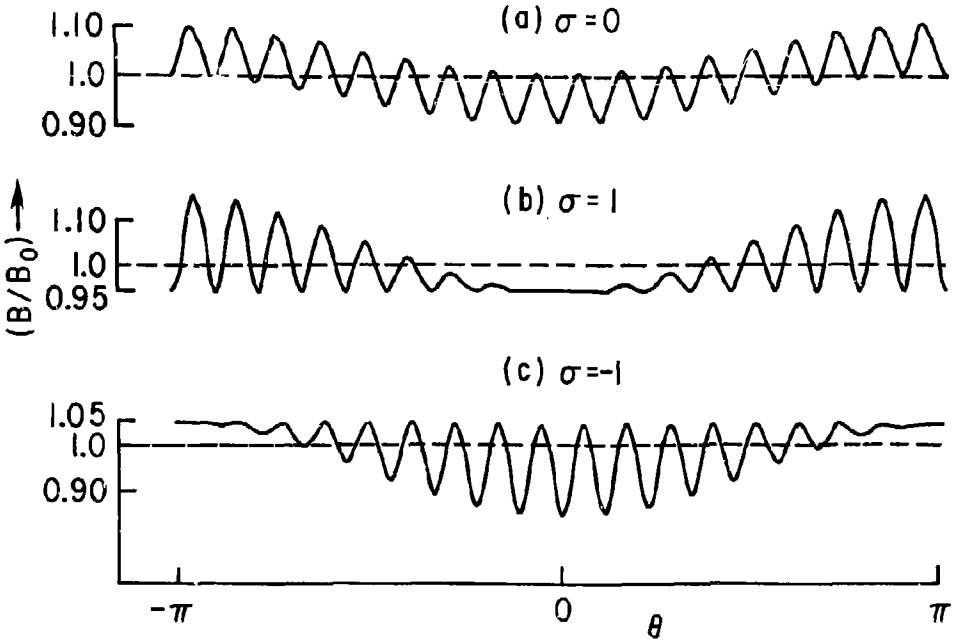

Fig. 1

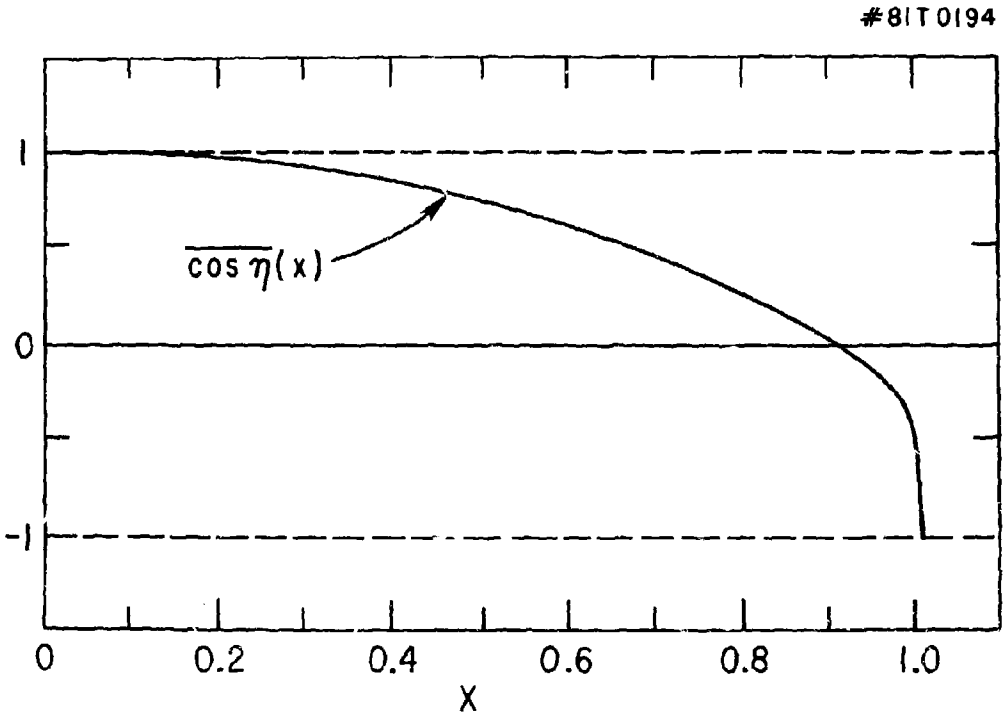

Fig. 2

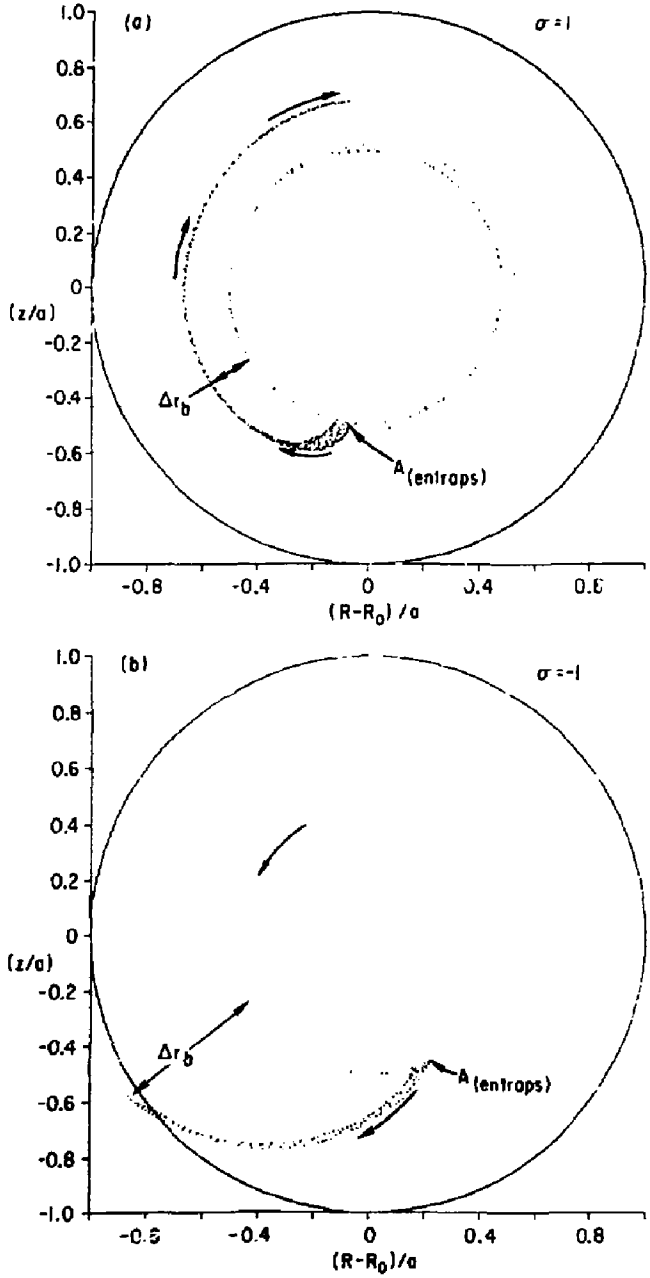

Fig. 3

#81T0196

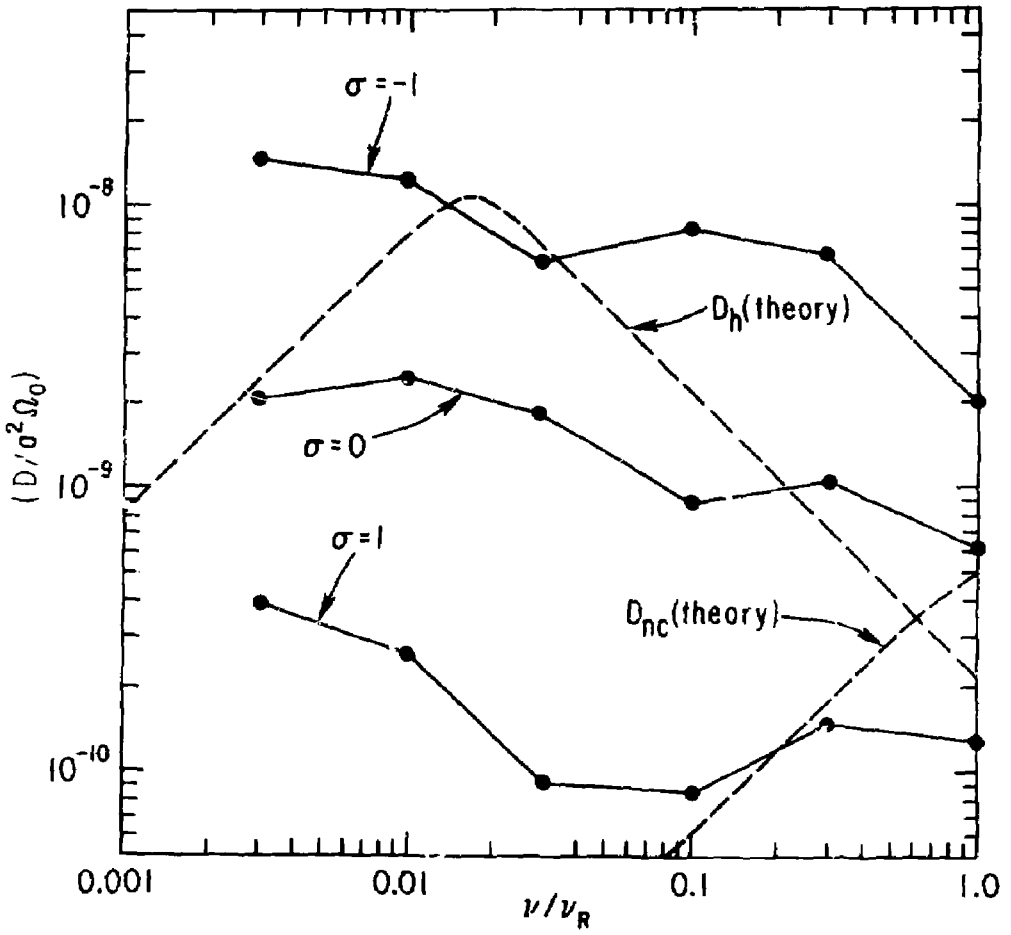

Fig. 4